Soils and Rocks

An International Journal of Geotechnical and Geoenvironmental Engineering

www.soilsandrocks.com

ISSN 1980-9743
ISSN-e 2675-5475

Proposed analytical method for predicting induced subsidence generated by dynamic compaction

Tennison Freire de Souza Junior[1#], Sidnei Helder Cardoso Teixeira[1], Alessander Christopher Morales Kormann[1]

Case Study

Keywords
Induced subsidence depth
Dynamic compaction
Frictional cohesive soils
Predictive model

Abstract

Dynamic compaction is a soil improvement method in which the soil is densified by multiple impacts of a heavy rammer in contact with the ground. Through this procedure, the natural soil increases its shear strength, stiffness, and density, and reduces the potential for swelling, hydraulic conductivity, and susceptibility to liquefaction. During the improvement process, soils undergo induced settlements until they stabilize after a certain number of blows. This process is monitored by the relationship between the compaction energy and the vertical displacement, which generally exhibits a hyperbolic trend that varies mainly as a function of density, as well as the magnitude of the energy, the soil type, the degree of saturation, and the rammer's contact area. Therefore, the objective of this article is to propose a predictive model for induced subsidence based on a hyperbolic equation derived from tests conducted on a frictional cohesive soil typical of Rio Grande do Sul. The results indicated that the model, when calibrated with the parameters λ_{DS} (dynamic displacement modulus) and ρ_{max} (Maximum variation of induced subsidence), satisfactorily reproduced the induced subsidence curves observed in the field, making the proposed formulation suitable for both design-stage predictions and field control of dynamic compaction operations.

1. Introduction

Dynamic compaction is a ground improvement method that involves percussive blows with a tamper weighing between 5 and 40 tons, dropped from a height of 10 to 40 meters, enabling compaction of various geotechnical materials to depths ranging from 4 to 10 meters on average (Hamidi, 2014; Han, 2015). This soil improvement method is frequently used in various countries around the world for road, airport, port, industrial, and building infrastructure projects (Hamidi, 2014; Souza Junior & Pasqual, 2021). It is suitable for loose and fully saturated soils, saturated free-draining soils, silts with a plasticity index lower than 8, and clayey soils with low saturation (moisture content below the plastic limit) (Han, 2015).

Historically, compaction-based ground improvement was employed without formal procedures in ancient Chinese and Roman civilizations. However, in 1970, the company Technique Louis Menard introduced the widely recognized "Heavy Compaction" (also known as "Heavy Tamping") as a soil improvement technique. Initially, this method targeted ballast deposits or natural sandy gravel soils, but it was later extended to saturated clay and alluvial soils. Consequently, the technique became known as "dynamic consolidation" (Menard & Broise, 1975). Currently, this method is frequently used for soil improvement in countries in the Middle East, Europe, Asia, and North America.

Specifications for tampers, heights, and distances between compaction points vary according to the desired improvement depth, which is defined based on design needs. Studies with varied tampers and drop heights have been conducted by researchers such as Gambin (1983), Mayne et al. (1984), Feng et al. (2011), Hamidi (2014), and others. Slocombe (2013) highlights that clayey soils behave more complexly than granular soils due to pore pressure generation caused by dynamic loading, with behavior differences depending on the water table level. If the water table is high (within 2 meters of the surface), it can affect the effectiveness of the method, making dewatering techniques necessary (Han, 2015).

The induced subsidence caused by dynamic compaction accounts for a portion of the improvement depth, making its understanding relevant for assessing the extent of the method. Mayne et al. (1984) suggested that induced subsidence measurements could be used to select the ideal number of blows and estimate the average induced subsidence depth caused by dynamic compaction. A summary of induced subsidence depths plotted on a site plan helps identify anomalous areas that may require additional treatment.

#Corresponding author. E-mail address: tennisongeotec@gmail.com
[1]Universidade Federal do Paraná, Departamento de Engenharia Civil, Curitiba, PR, Brasil.

Submitted on September 1, 2025; Final Acceptance on January 5, 2026; Discussion open until November 30, 2026.

Editor: Renato P. Cunha

https://doi.org/10.28927/SR.2026.014625

In current practice, the monitoring of induced subsidence caused by compaction is presented in the geotechnical literature based on empirical equations found in the works of Oshima and Takada (1994, 1997), Souza Junior & Pasqual (2021), among others. These models simulate physical behavior through mathematical adjustments, without necessarily considering analytical behavior under large deformations. Empirical models are based on calibrations obtained through field tests without considering the theoretical conditions of the model, especially when dealing with tropical soils.

Recent studies have continued to investigate dynamic compaction mechanisms, focusing on optimization of compaction parameters (Bayat et al., 2024), large-scale field testing and vibration behavior (Du et al., 2025), and the influence of tamper mass and drop height on induced subsidence (Li et al., 2025). While these studies provide valuable insights into compaction performance and soil response, they remain largely experimental or numerical in nature and do not offer a simple analytical framework for predicting induced subsidence evolution during field operations.

The analytical framework for simulating the behavior of dynamic compaction presents a reliable alternative to computational methods. Therefore, this article proposes an analytical approach for estimating subsidence caused by dynamic compaction, based on field investigations carried out in a clayey lateritic soil in Rio Grande do Sul, Brazil.

Although empirical models for predicting induced subsidence in dynamic compaction have been widely used in practice, they are generally derived from site-specific datasets and calibrated for particular soil types, compaction energies, and equipment configurations. As a result, their applicability outside the original conditions of calibration is limited. This limitation becomes more pronounced in frictional-cohesive and lateritic soils, where soil structure, cementation, and moisture-dependent behavior differ significantly from the granular soils on which most empirical formulations are based. Consequently, empirical approaches often fail to provide consistent predictions when applied to tropical and subtropical soils or under varying environmental conditions. These limitations highlight the need for alternative approaches that retain physical interpretability while reducing dependence on site-specific empirical correlations.

Unlike existing empirical formulations for predicting induced subsidence in dynamic compaction, which are typically site-specific and based solely on curve fitting of field data, the proposed model introduces an analytical formulation grounded on energy accumulation and asymptotic displacement behavior. The model requires only two physically interpretable parameters, allowing the evolution of induced subsidence to be described in a continuous and consistent manner. This approach enables real-time monitoring of the compaction process, the definition of objective stopping criteria, and applicability to frictional-cohesive lateritic soils, which are not adequately addressed by current empirical charts and correlations.

In addition, the proposed formulation offers a computationally efficient alternative to numerical methods, as it does not require complex constitutive models or extensive parameter calibration, making it suitable for both design-stage predictions and field control during dynamic compaction operations.

2. Background

The high-energy compaction can induce the formation of craters with depths ranging from 1.0 to 1.5 m. The crater depth should be limited to the height of the tamper plus 0.3 m to ensure safety and ease of the compaction operation. When the crater depth becomes too great, the compaction process should be divided into two or more phases (Han, 2015).

The Figure 1 illustrates the application of the dynamic compaction method. As can be seen, the tamper (W) is released from a height (H) using cables or by free fall onto the ground. The soil responds to the improvement by forming a crater (induced subsidence), while the impact also allows dynamic stresses to propagate down to a maximum improvement depth (D).

Even today, estimating soil densification efficiency in dynamic compaction remains a challenge. Existing methods often fail to adequately account for the distinct contributions of Tamper (W) and drop height (H) (Li et al., 2025). Another aspect that has been extensively studied is the optimization of dynamic compaction conditions, specifically the relationships between influence radius, densification bulb, tamper, and drop height, using a metaheuristic approach (Bayat et al., 2024).

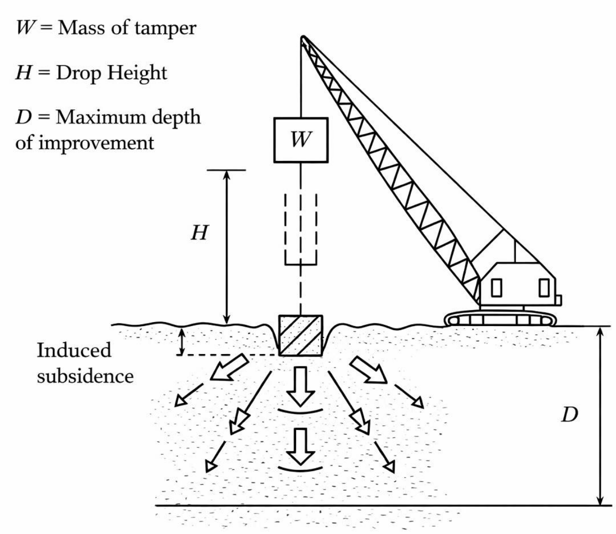

Figure 1. Dynamic compaction method. Lukas (1995).

Recent research on red clays using the same energy but with heavier tamper and lower drop heights has shown greater induced subsidence depths and more pronounced plastic deformation. Specifically, in this study, it was observed that the heavier tamper caused impact stress with a longer duration, increasing both the stress wavelength and energy propagation (Li et al., 2025). Other researchers have demonstrated that the vibration amplitudes generated by dynamic compaction stabilize after a certain number of blows, showing trends similar to those of induced subsidence (Du et al., 2025).

Rollins & Kim (2010) proposed empirical formulations to estimate the induced subsidence in soils with low degrees of saturation (S_r) after the application of dynamic compaction energy, considering the drop height, tamper width and weight, number of blows, drop spacing, and tamper contact pressure. The induced subsidence represents an important constitutive portion of the improvement depth achieved by the method. From the perspective of classical mechanics, the monitoring of improved depth can be carried out based on potential energy (Mayne et al., 1984; Lukas, 1995) or the law of conservation of linear momentum (Mikasa et al., 1988; Oshima & Takada, 1994, 1997).

Technical literature offers a wide range of empirical formulations for estimating the depth of influence in sedimentary deposits, collapsible soils, solid waste, and other materials. These formulations have been proposed by various researchers, including, Menard & Broise (1975), Charles et al. (1978), Leonards et al. (1980), Mitchell (1981) Varaksin (1981), Smoltczyk (1983), Mayne et al. (1984), Qian (1987), Van Impe (1989), Luongo (1992), Rollins & Rogers (1994), Lukas (1995), Fei et al. (2002), Yasrobi & Asghari (2004), Feng et al. (2011), Souza Junior & Pasqual (2021), among others.

To model the shapes of induced subsidence and estimate their depths, some researchers have used numerical models coupled with constitutive soil models in one, two, and three dimensions. Examples include Chow et al. (1992) in 1D; Qian (1987), Pan & Selby (2001), Lee & Gu (2004), López-Querol et al. (2007), Mostafa (2010), Ghanbari & Hamidi (2015), Wang et al. (2017), and Du et al. (2019) in 2D; Hamidi (2014), Mehdipour & Hamidi (2017), Moon et al. (2019), and Wang et al. (2019) in 3D. However, no studies to date have applied these formulations specifically to subtropical and tropical frictional-cohesive soils, and these are numerical applications that require computational cost, in addition to requiring an expressive amount of parameters that provide a representative description of the soil's plastic and volumetric deformations.

During dynamic compaction, the typical behavior of subsidence induced by tamper impact varies according to the energy accumulated from the series of blows. which is consistent with a hyperbolic curve similar to that expressed by Kondner & Horner (1965) and Kondner (1963). In these studies, the hyperbolic graph was able to reproduce the nonlinear stress-strain curves of clays and sands in triaxial tests with satisfactory accuracy. The hyperbolic formulation proposed by Kondner can be seen in Equation 1:

$$\sigma_1 - \sigma_3 = \frac{\varepsilon}{\alpha + \beta\varepsilon} \tag{1}$$

In the proposed hyperbolic equation, the curve geometry is developed from parameters alpha and beta. The α parameter is associated with the stiffness in the stress-strain behavior of triaxial tests, that is, the slope of the hyperbola at low axial strains. Regarding β parameter beta, from a mathematical standpoint, it represents the sample's asymptotic strength ($q_{E\to\infty}$).

3. Proposed method for induced subsidence depth simulation

The induced subsidence curves depend on both the compaction energy and the soil type, the parameters α and β are sensitive to the test conditions (N, H, and W), as well as to soil properties (e.g., degree of saturation, grain size distribution, void ratio, etc.). The compaction energy is calculated using the potential energy calculated (E) based on classical mechanics, such that the improvement is controlled by the accumulated potential energy (E_{ac}) in the soil through Equation 2:

$$E_{ac} = \sum_{i=0}^{n} E = N.W.H.g \tag{2}$$

Based on Kondner & Horner (1965) and Kondner (1963), equations 3 and 4 express the mathematical relationship between dynamic plastic displacement and impact energy accumulated.

$$\frac{\rho}{E_{ac}} = \frac{1}{\alpha' + \beta' E_{ac}} \tag{3}$$

$$\rho = \frac{E_{ac}}{\alpha' + \beta' E_{ac}} \tag{4}$$

The equilibrium of impact-induced subsidence occurs at large deformations. At the beginning of the hammer impact sequence, the increment of induced subsidence increases due to the progressive rearrangement of the soil grains, and then gradually decreases until it becomes null (Equation 5), at which point the soil has reached the intended improvement condition.

$$\frac{\partial(\rho)}{\partial E_{ac}} = 0 \tag{5}$$

The proposed hyperbolic model is calibrated based on two parameters: λ_{Ds} and ρ_{max}. The parameter λ_{Ds} is the dynamic subsidence modulus, i.e., the early-stage displacement increment caused by the first tamper blows and parameter ρ_{max} represents the total induced subsidence, or the full displacement range over the compaction process.

Conceptually, the value of λ_{DS} is obtained at $E_{ac} = 0$ through the partial derivative of ρ with respect to E_{ac}, which is expressed by Equation 6:

$$\left[\frac{\partial(\rho)}{\partial E}\right]_{E=0} = \frac{1}{\alpha'+\beta'E} - \frac{\beta' E_{ac}}{\left(a'+\beta' E_{ac}\right)^2} \rightarrow \alpha' = \frac{1}{\lambda_{DS}} \qquad (6)$$

The ρ_{max} value is closely related to subsidence stabilization. As shown in Equation 7, the parameter ρ_{max} also defines the limit of induced subsidence variation at infinite energy input ($E_{ac} = \infty$):

$$\lim_{E\to\infty} E(\rho) = \lim_{E\to\infty} \frac{\rho}{\frac{1}{\lambda_{DS}} + \frac{E_{ac}}{\Delta\rho}} \rightarrow \beta' = \frac{1}{\rho_{max}} \qquad (7)$$

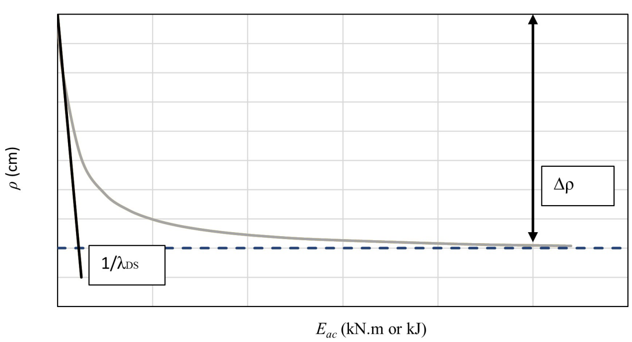

Figure 2. Hyperbolic model of evolution of Induced subsidence (ρ) vs Impact Energy (E_{ac}).

Finally, Equation 8 summarizes the proposed theory in a single and simplified formulation of induced subsidence behavior. This equation can be used both to simulate the induced subsidence curve during dynamic compaction and to estimate its equilibrium value. It can be easily solved using iterative numerical techniques, such as a solver with the least squares method. However, it is essential that the model represents a condition in which the induced subsidence has stabilized.

$$\rho = \frac{E_{ac}}{\frac{1}{\lambda_{DS}} + \frac{E_{ac}}{\rho_{max}}} \qquad (8)$$

In this study, since the contact area was kept constant, this variable is not included in the formulation.

The parameters can be determined by estimating the value of λ_{DS} and ρ_{max} (Figure 2), iteratively adjusting until the best visual fit of the curve is achieved. Alternatively, a statistical approach can be employed using spreadsheet software and the solver tool, applying the least squares method to optimize the parameter set. One method of obtaining them is by using a numerical solver tool with the least squares method.

4. Materials and methods

4.1 Soil characteristics in the experimental field

Figure 3 illustrates the location of the experimental field, whose geographical coordinates are 28°13’35”S, 52°23’12”W. This field contains cohesive-frictional soil with a homogeneous residual nature, derived from the decomposition of basaltic (igneous) rocks and sandstones (sedimentary), according to Ruver (2011) and Faro (2014). Sachetti et al. (2014), using X-ray fluorescence spectrometry, concluded that the soil resulted from the

(a) (b)

Figure 3. Experimental Field in Passo Fundo: (a) in loco view; (b) upper view.

weathering of acidic igneous rocks known as rhyodacites (rhyolites + dacites). Streck et al. (2002) classified the soil in the Passo Fundo region as a typical "Dystrophic Red Latosol," part of the "Passo Fundo Formation."

From a geological perspective, the region of Passo Fundo/RS is part of the Phanerozoic eon, Mesozoic era, and Cretaceous period (see Figure 4). It is characterized by acidic lava flows ranging from rhyodacites to rhyolites, with a vitrophyric matrix containing phenocrysts; intermediate to acidic flows, from rhyodacites to rhyolites, mesocratic, microgranular to vitrophyric, commonly displaying spherulitic textures (carijó-type), strong tabular jointing at the top of the flows and massive structure in the central portion, frequent flow folds and autobreccias, vesicles predominantly filled with chalcedony and agate—the source of the region's mineralizations—and the Tupanciretã Formation (fine quartz-rich sandstone, paraconglomerate, and conglomeratic sandstone, deposited in a continental environment.

Souza Junior et al. (2019) classified the soil as lateritic clay (*LG'*) by the *MCT* method for tropical soils. Lateritic soils result from intense weathering of the parent rock, with leaching of bases and part of the silica, organic matter decomposition, and a predominance of kaolinite coated with iron and aluminum oxides and hydroxides, which give the material a cemented appearance. (Nogami & Villibor, 1995)

Carretta (2018), comparing this soil to data from Rizzon (2016) and Thomé et al. (2017), found that the S_r varied between 72% and 75.7%, the initial void ratio (e) ranged from 1.20 to 1.28, and porosity (η) from 54% to 55%. Several studies have reported the properties and parameters of this soil. Dalla Rosa et al. (2004) characterized it granulometrically and found 2% medium sand, 25% fine sand, 8% silt, and 65% clay. Ruver (2011) obtained 0.45% coarse sand, 2.06% medium sand, 18.57% fine sand, and 78.91% fines (59% clay and 19.9% silt). Carretta (2018) conducted granulometric characterization of undisturbed samples, resulting in 35% sand and 65% fines (60% clay and 5% silt).

Ruver (2011) noted that based on granulometry and plasticity index (*PI*), the frictional cohesive soil of the Passo Fundo experimental field (*UPF*) could be classified as A-5-7 by the American Association of State Highway and Transportation Officials (AASHTO, 1991) and *CL* (Clay with Low plasticity) by the Unified Soil Classification System (*SUCS*) (ASTM, 2017).

Table 1 shows a comparison of properties reported by different authors. The values show little variability, although Dalla Rosa et al. (2004) reported higher values for the liquid limit (*LL*) and plasticity index (*PI*). Based on the data presented in Table 1 and the grain size distribution of the current soil, it is noted that its properties and geotechnical parameters do not allow it to be classified according to the chart proposed by Lukas (1995). It is observed that this formation has in situ hydraulic conductivity corresponding to zone 1, grain size distribution of zone 2, and a plasticity index of zone 3—therefore, a type of soil not covered in the technical literature.

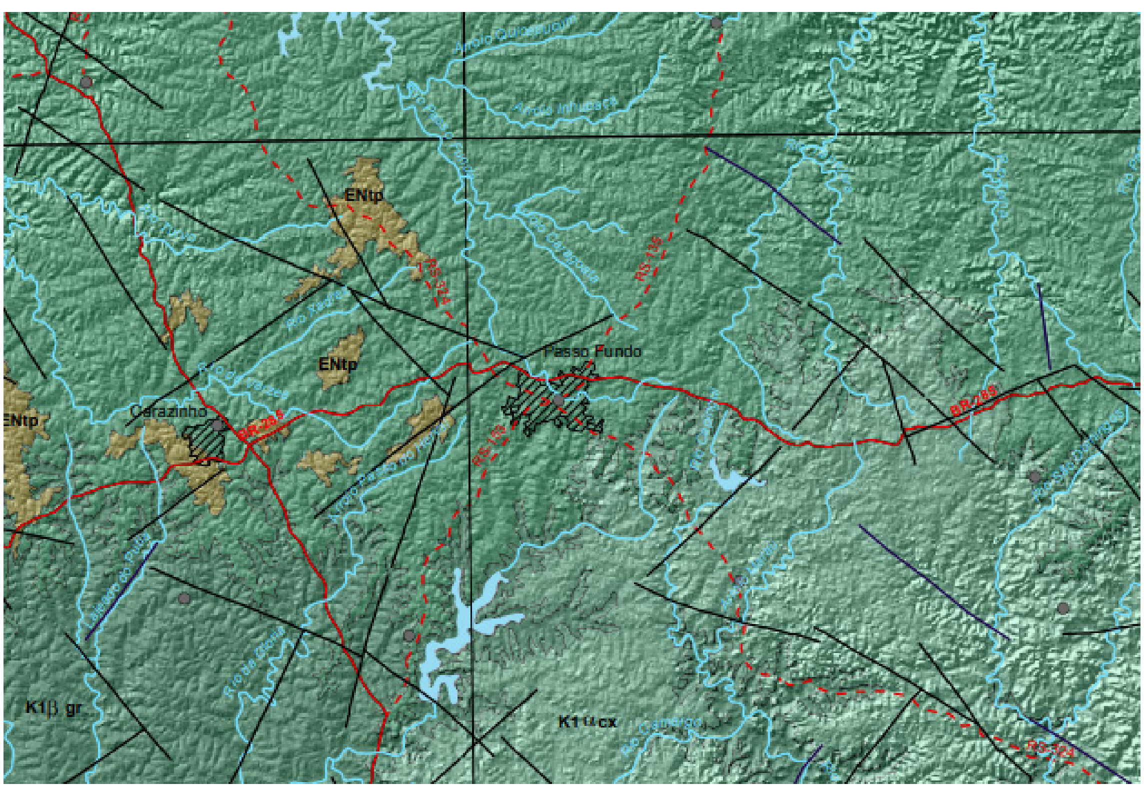

Figure 4. Geological Map of Rio Grande do Sul. (SGB,2025).

Table 1. Comparison between the frictional cohesive properties and parameters of the soil in Passo Fundo - RS.

Properties	Carretta (2018)	Ruver (2011)	DallaRosa et al. (2004)	Rizzon (2016) and Meneghetti et al. (2009)
Average natural moisture - ω (%)	35	28.87	27-29	34
Specific grain weight - γ_g (kN/m³)	---	26.7	26.5-28.2	26.7
Plastic limit – *PL* (%)	31	32 ± 4	35	42
Liquid limit – *LL* (%)	42	41	55	53
Plasticity index – *PI* (%)	11	9± 4	20	11

Dalla Rosa et al. (2004) concluded that *LL*, *PL*, *PI*, and grain size curves were similar up to approximately 6 meters in depth. Faro (2014) conducted five Cone Penetration Tests (*CPT*) at different locations in the field, following ASTM D5778 (ASTM, 2012). The tests indicated that soil is homogeneous stratification up to 15 meters, with only slight variations in cone tip resistance by *CPTu*s. The water table was not detected, suggesting significant depth, implying that dynamic compaction in this area is unlikely to increase pore pressure or manifest dynamic consolidation behavior (Menard & Broise, 1975).

4.2 Procedures and tests

Lukas (1995) established that the static contact pressure should be limited between 40 kPa and 75 kPa, since excessive pressure in sedimentary soils could cause punching or grain breakage, while low pressure might not yield significant improvement. Han (2015) noted that tampers are typically made of concrete or steel, with contact areas ranging from 3 to 6 m², depending on soil type.

The tampers (Weight or hammer) used in the research had different masses and geometries. First tamper, 55 kN with static contact pressure of 48.3 kPa (Figure 5a). Second tamper, 100 kN (55 kN + 45 kN coupling) with a static contact pressure of 88.7 kPa (Figure 5b). Both tampers had a base diameter of 1.20 m. In experimental tests, the Compaction points were spaced at a minimum 3D distance based on Lukas (1995).

To enable the lifting and release of the tamper, a 250 kN crane was used for the studies involving cables, and a 600 kN crane was used for the free-fall studies. The use of different cranes was chosen due to the whiplash effect caused by the rapid release of the tamper in the free-fall scenario.

Dynamic compaction studies were conducted by varying the tamper mass (*W*), drop height (*H*), and number of blows (*N*), with the aim of evaluating the influence of these parameters on the behavior of the induced subsidence hyperbola. Four dynamic compaction tests were performed with cables based on the characteristics in Table 2 and localized in the Figure 6.

Table 3 presents the free-fall test matrix with seven studies, where the tamper was constant and the height and number of blows were varied. Some tests were conducted under rainy conditions, which may have affected the degree of saturation and subsequent subsidence behavior.

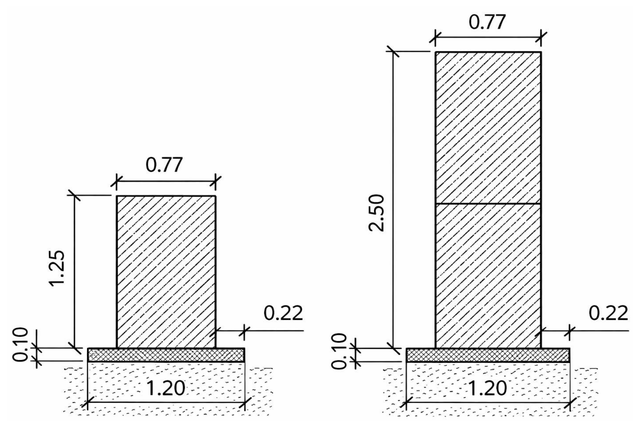

Figure 5. Geometric specifications of tamper (in meter): (a) 55 kN; (b) 100 kN (Rizzon, 2016).

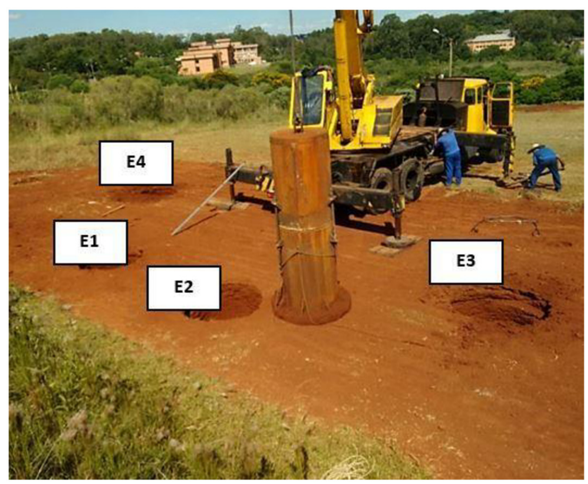

Figure 6. Experimental field in Passo Fundo – RS (Rizzon, 2016).

5. Results and discussions

As shown in Figure 7 the simulated curves generated using the proposed method exhibit strong agreement with the observed behavior of ρ vs E. In general, the greater the compaction energy applied, the larger the increments of induced subsidence observed.

Table 2. Characteristics of the tests performed in prototypes (using cables).

Tests	Parameters		
	W- Tamper (kN)	*H*-Height (m)	*N* – Number of Blows
EC1	55	3.0	40
EC2	55	3.0	40
EC3	100	3.0	15
EC4	100	1.5	20

Table 3. Characteristics of the tests performed in the free fall.

Tests	Parameters		
	W -Tamper (kN)	*H* - Height (m)	*N* - Blows
TFF1*	55	9.0	4
TFF2*	55	6.0	4
TFF3*	55	6.0	8
TFF4*	55	6.0	8
TFF5	55	8.0	4
TFF6	55	12.0	3
TFF7	55	6.0	5

*tests performed in raining conditions.

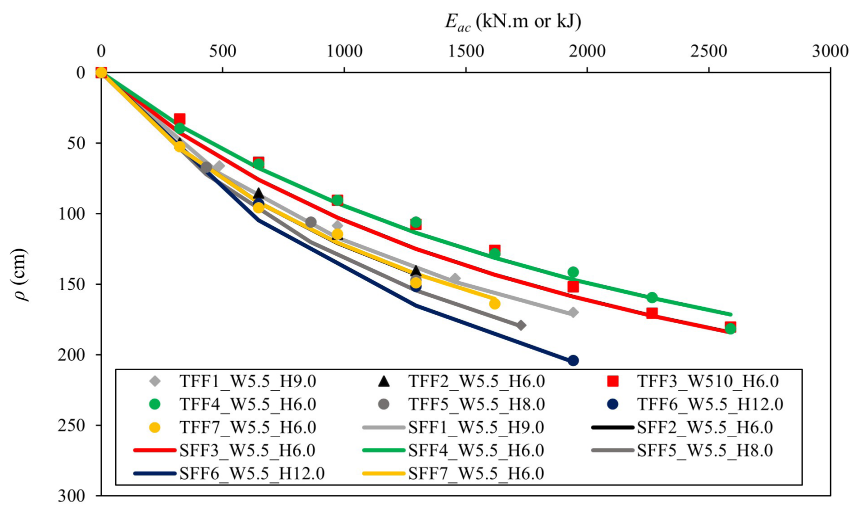

Figure 7. Comparative study between subsidence responses induced versus impact energy (*E*) obtained from field tests (TFF) and numerical simulation (SFF) - Free fall.

Regardless of the energy applied, the induced subsidence response was closely aligned with the results from the experimental field tests. These responses suggest that the hyperbolic model is capable of simulating the induced subsidence from dynamic compaction, but it is important to note that the field experimental studies did not reach the asymptote of full densification. This behavior suggests that higher energy levels would be required to achieve maximum density.

The present soil experienced greater induced settlements during the initial tamper blows due to the collapse of voids in the formation and the loss of shear strength resulting from the breakdown of natural cementation (Consoli et al., 2020). As dynamic compaction progressed, the macropores were initially collapsed (Consoli et al., 2020), promoting new particle rearrangements (Hamidi, 2014), as well as the dissipation of pore pressure through the cracks generated in the soil (Menard & Broise, 1975). Consequently, this process resulted in a volumetric reduction of the soil.

Given the soil's high saturation index (between 72% and 75.7%), along with its drainage conditions and the formation of percolation paths generated by tamper impacts (Menard & Broise, 1975), it is likely that, for the same energy level, there is a consistent pattern in subsidence behavior. As observed in Figure 7, tests conducted on sunny days with accumulated compaction energy showed greater induced subsidence compared to rainy days. This may be related to the high degree of saturation of the base soil, such that the voids that were previously filled with air collapsed and were subsequently filled with water.

In Figure 8, two test results deviate from the linear trend between λ_{DS} and ρ, although they remain within a specific cluster. This variability may be linked to rainfall effects (altering the degree of saturation) and material heterogeneity (such as grain size distribution or initial compaction).

Under the free fall condition, it was possible to correlate the independent parameters (N, W, and H) with the dependent parameter $1/\rho_{max}$. The analysis resulted in a moderate correlation (R^2 equal to 0.7101). The height of tamper (W) had a null effect in this case, as all free-fall tests were conducted using the same tamper. The regression model for $1/\rho_{max}$ is presented in Equation 9:

$$\frac{1}{\rho_{max}} = 0.0029 - 5.7x10^{-5}H + 0.000132N \quad (9)$$

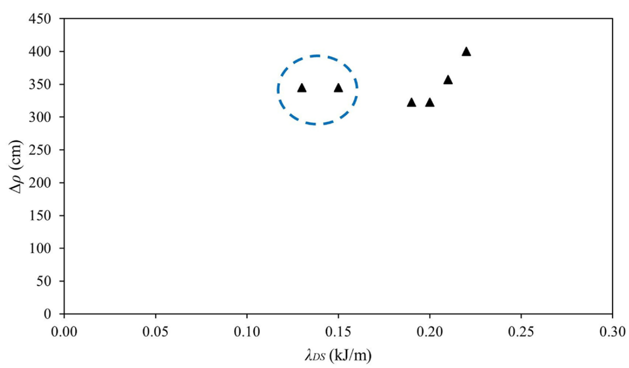

Figure 8. Relationship of calibration parameters λ_{DS} and ρ in dynamic compaction free fall.

Figure 9 presents the results of dynamic compaction tests conducted with tamper of 55 kN and 100 kN, and drop heights of 3.0 m and 1.5 m. It can be observed that for the heavier tamper (W = 100 kN), represented by tests TC3_W10_H3.0 and TAn important aspect is that there was repeatability in the behavior of the curves in tests TC1 and TC2, which indicates the homogeneity of the soil being worked on, as well as consistency in the test conditions. C4_W10_H1.5, the induced subsidence depth appears to be independent of the drop height.

This behavior suggests the existence of a threshold for the impact energy per blow, beyond which further increases in drop height do not lead to significant additional subsidence. In practical terms, this may imply that increasing the drop height above a certain level may not be effective for enhancing soil densification. However, this hypothesis requires further validation through additional experimental data to confirm the existence of a maximum induced subsidence limit under high-energy impacts.

Using another multiple linear regression model, the parameters N, W, and H were again correlated with $1/\rho_{max}$. In the present study, the drop height (H) was a parameter with low variation within the sample set, which consequently resulted in low significance and was therefore disregarded.

$$\frac{1}{\rho_{max}} = 0.005 - 3x10^{-5}W + 7.67x10^{-21}N \quad (10)$$

The model showed a high level of correlation ($R^2 = 0.943$). It is worth noting that the number of blows (N) was not statistically significant in this case, likely due to the small variation in the number of blows between tests.

After simulating the subsidence curves (see Figure 10), the parameters λ_{DS} and ρ_{max} were plotted in Figure 10.

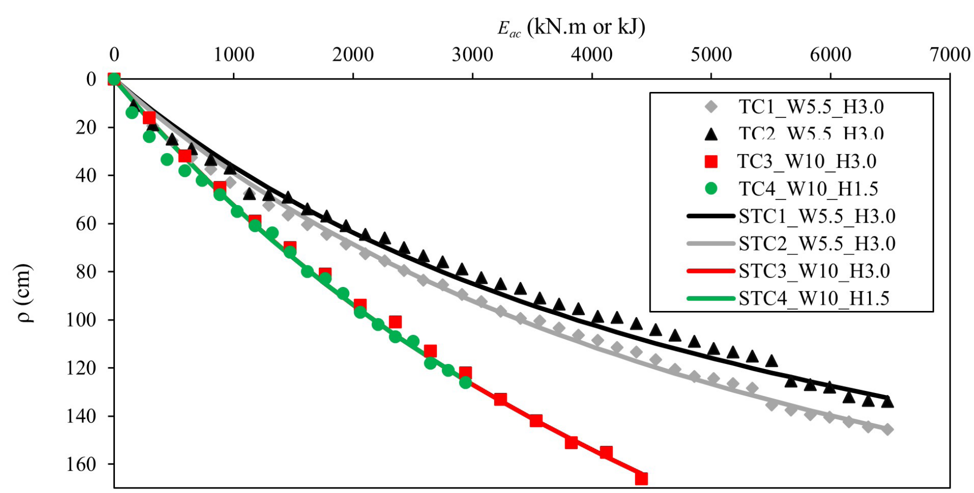

Figure 9. Comparative study between subsidence responses induced versus impact energy (E) obtained from field tests (TC) and numerical simulation (STC) – Cable test.

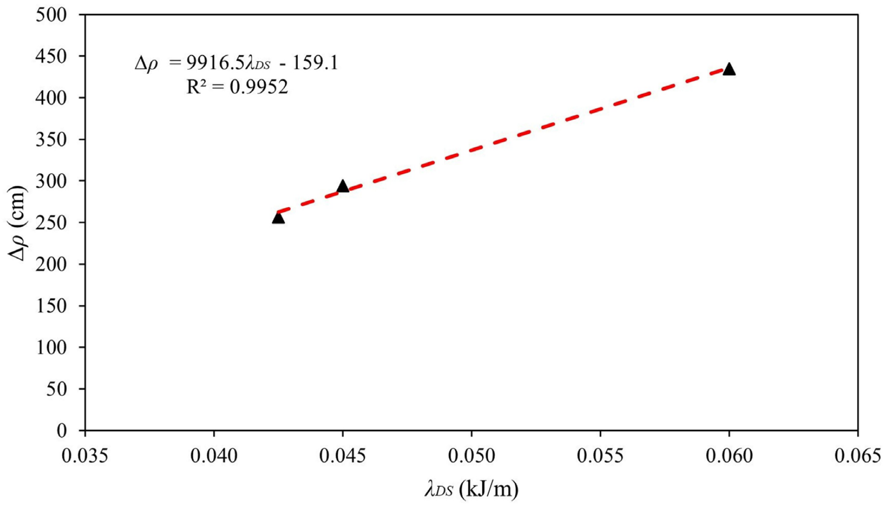

Figure 10. Relationship of calibration parameters λ_{DS} and ρ_{max} in dynamic compaction with cables.

An excellent linear correlation was observed ($R^2 = 0.9952$), indicating a consistent subsidence trend under cable-based compaction conditions.

The results indicate that tamper mass plays a dominant role in controlling induced subsidence, particularly under cable-based compaction conditions, whereas increasing drop height beyond a certain threshold yield diminishing returns in terms of additional settlement. This finding suggests the existence of an optimal energy per blow, beyond which further increases in height do not significantly enhance soil densification. Such behavior is consistent with the observed asymptotic nature of the subsidence curves and has important implications for compaction design.

A qualitative sensitivity analysis indicates that the proposed model parameters exhibit different levels of influence on the predicted induced subsidence. The parameter λ_{DS} primarily governs the initial slope of the subsidence–energy curve, reflecting the soil's early-stage deformability, while $\Delta\rho$ controls the asymptotic displacement reached at large energy levels. Variations in drop height and tamper mass mainly affect $\Delta\rho$, whereas the number of blows has a secondary influence under the tested conditions. These trends are consistent with the observed regression results and highlight the physical meaning of the calibration parameters.

The agreement between measured and simulated induced subsidence curves suggests that the proposed model provides a satisfactory representation of field behavior. However, discrepancies may arise from measurement uncertainty, local soil heterogeneity, variations in moisture content, and simplifications adopted in the formulation, such as constant contact area and uniform energy transfer. The observed scatter in the calibration parameters reflects these sources of uncertainty. Despite this, the model maintains consistent trends, indicating robustness with respect to typical field variability

The consistency of the observed trends across different test configurations suggests that the model is relatively robust with respect to typical field variability, provided that parameters are calibrated using representative early-stage subsidence data.

The proposed hyperbolic formulation assumes that induced subsidence evolves asymptotically with increasing accumulated impact energy. Therefore, the model is most appropriate for conditions in which the compaction process reaches or approaches stabilization. At very low compaction energies, the model may overestimate early-stage subsidence due to insufficient soil rearrangement. Conversely, at extremely high energy levels, soil crushing, excessive crater formation, or localized failure mechanisms may occur, which are not explicitly captured by the present formulation.

Potential sources of error in the proposed model include uncertainties in field measurements of induced subsidence, variability in soil properties (such as degree of saturation and cementation), and simplifications related to constant contact area and uniform energy transfer. These sources of error can be mitigated through repeated measurements, careful control of field-testing conditions, and calibration of model parameters using early-stage subsidence data. Additionally, the use of statistical fitting techniques, such as least squares optimization, contributes to reducing subjective bias in parameter estimation.

The validation of the proposed model in this study is based on an extensive experimental program conducted on a frictional-cohesive lateritic soil, which represents a soil class not adequately covered by existing empirical dynamic compaction models. While the results demonstrate a consistent ability of the model to reproduce induced subsidence behavior under different compaction configurations, the authors acknowledge that additional validation using different soil types, such as granular soils, highly plastic clays, and collapsible deposits, is necessary to fully assess the model's general applicability. Such investigations are beyond the scope of the present study and are recommended as future research.

Compared to empirical approaches such as those proposed by Oshima and Takada (1994, 1997) and Souza Junior & Pasqual (2021), which rely on site-specific calibration, the present model provides a general analytical framework capable of capturing the asymptotic nature of induced subsidence with increasing energy input. This distinction is particularly relevant for tropical frictional-cohesive soils, where empirical formulations derived from granular or temperate-climate soils may not be applicable.

Although the experimental program was conducted on a single soil type, the test matrix included variations in environmental conditions, particularly rainfall during free-fall tests, which affected the degree of saturation of the soil. The results indicate that higher moisture conditions tend to reduce the magnitude of induced subsidence for similar energy levels, likely due to reduced air-filled void collapse and increased pore water presence. This observation highlights the sensitivity of the proposed model parameters to environmental conditions, particularly soil moisture, and reinforces the importance of proper parameter calibration for each site condition.

Compared to existing empirical formulations, which are often derived from specific soil conditions and compaction configurations, the proposed model offers a unified analytical framework based on energy accumulation and asymptotic behavior. While empirical models may provide direct estimates under conditions similar to those from which they were derived, their applicability under varying environmental conditions is limited. In contrast, the present formulation allows recalibration of physically interpretable parameters to account for changes in soil moisture and compaction conditions, improving adaptability without increasing computational complexity.

6. Conclusion

The present study proposed a hyperbolic analytical model to simulate the behavior of induced subsidence during the application of the dynamic compaction method. The investigations were based on drop tests—both free-fall and cable-assisted—conducted in an experimental field on a frictional-cohesive lateritic soil typical of Rio Grande do Sul, Brazil.

In general, under both free-fall and cable-assisted conditions, the proposed hyperbolic model was able to satisfactorily reproduce the induced subsidence behavior observed in the field, demonstrating its suitability as a predictive and monitoring tool for dynamic compaction processes.

Based on the experimental matrix and the soil formation analyzed, it was observed that the calibration parameters λ_{DS} and $\Delta\rho$ exhibited a linear trend across different combinations of number of blows (N), tamper mass (W), and drop height (H) when compaction was performed using cables. This trend was not consistently observed under free-fall conditions, which may be attributed to soil heterogeneity and variations in environmental conditions.

Multiple regression analyses indicated a strong correlation between the compaction parameters N and H and the prediction of $\Delta\rho$ for both cable-assisted and free-fall conditions, highlighting the relevance of these parameters in controlling induced subsidence evolution.

From a practical standpoint, the proposed model can be directly integrated into dynamic compaction field control procedures by monitoring induced subsidence after each blow or sequence of blows. The calibrated parameters allow engineers to define objective stopping criteria, optimize the selection of tamper mass and drop height, and reduce unnecessary energy expenditure, thereby improving operational efficiency and cost-effectiveness.

In addition, the model may be incorporated into design-stage analyses to support preliminary estimates of expected subsidence evolution and improvement efficiency, as well as into numerical simulations as a simplified constitutive representation of densification behavior. By enabling real-time calibration and interpretation of subsidence trends, the model also supports adaptive control of the compaction process and informed decision-making during field operations.

Although the proposed formulation demonstrated consistent performance for the studied soil and test configurations, its general applicability should be further investigated. Future research should focus on extending model validation to a broader range of soil types, including granular soils, highly plastic clays, collapsible soils, residual soils, and sedimentary deposits, under different climatic and environmental conditions. Additional studies should examine the influence of varying tamper geometries, contact areas, and dynamic compaction equipment scales on model parameters.

Another promising research direction is the integration of the proposed formulation with advanced constitutive models and numerical simulations, enabling its application in stress–strain analyses and performance-based design approaches. Finally, coupling the model with automated field monitoring systems may allow real-time parameter calibration and adaptive optimization of dynamic compaction operations.

Acknowledgements

The authors would like to thank CAPES for funding the research through the *PPGEC* (Civil Engineering Postgraduate Program) at *UFRGS* (Federal University of Rio Grande do Sul) and UFPR (Federal University of Paraná). We also extend our gratitude to the anonymous reviewers for their insightful comments and suggestions, which significantly improved the content of this article.

Declaration of interest

The authors declare that they have no known competing financial interests or personal relationships that could have appeared to influence the work reported in this paper.

Authors' contributions

Tennison Freire: conceptualization, methodology and writing - original draft preparation. Sidnei Teixeira: investigation, data curation, reviewing and validation. Alessander Kormann: writing - reviewing and editing.

Data availability

The data supporting the analyses and results of this study are available from the corresponding author upon request and as needed.

Declaration of use of generative artificial intelligence

Generative artificial intelligence tools were used exclusively for language refinement. The authors are fully responsible for scientific content, data interpretation, and conclusions.

List of symbols and abrevations

e	Void index
g	Gravitational acceleration
q	Desviatoric stress
AASHTO	American Association of State Highway and Transportation Officials
ASTM	American Society for Testing and Materials
CAPES	Coordination for the Improvement of Higher Education Personnel;
CPT	Cone piezometer test;
CPTu	Cone Penetration Test with pore pressure measurement
CL	Clay low plasticity
E	Impact energy or potential energy
E_{ac}	Accumulated potential energy
E_c	Energy compaction
H	Drop height
LG'	Lateritic clay soil
LL	Liquid limit
MCT	Miniature, Compacted, Tropical Soil Classification System
N	Number of blows
PI	Plasticity index
PL	Plastic limit
PPGEC	Civil Engineering Postgraduate Program
TC	Cable test
R^2	Determination coefficient
S_r	Degree saturation
SFF	Free fall simulation;
STC	Cable test simulation;
SUCS	Unified Soil Classification System
TFF	Free fall test
UPF	Passo Fundo University
UFPR	Federal University of Paraná
UFRGS	Federal University of Rio Grande do Sul
W	Tamper
α	Stiffness coefficient
α'	Dynamic displacement coefficient
β	Asymptotic shear strenght coefficient
β'	Asymptotic displacement coefficient
$\Delta_{\rho\, máx}$	Maximum variation of induced subsidence
γ	Bulk unit weight
γ_g	Specific grain weight
λ_{Ds}	Dynamic displacement modulus
ρ	Induced subsidence
$\rho_{máx}$	Maximum induced subsidence
σ_1, σ_3	Principal normal stress
ω	Average natural moisture

References

AASHTO M145. (1991). *Standard Specification for Classification of Soils and Soil-Aggregate Mixtures for Highway Construction Purposes*. AASHTO, Washington, USA.

ASTM D2487. (2017). *Standard Practice for Classification of Soils for Engineering Purposes*. ASTM, West Conshohocken, USA.

ASTM D5778. (2012). *Standard Test Method for Electronic Friction Cone and Piezocone Penetration Testing of Soils*. ASTM, West Conshohocken, USA.

Bayat, M., Saadat, M., & Hojati, A. (2024). Optimization of dynamic compaction procedure for sandy soils. *Civil Engineering Infrastructure Journal*, 57(1), 145-156.

Carretta, M.S. (2018). *Comportamento de um solo residual levemente cimentado: estimativa de capacidade de carga para estacas submetidas a esforços transversais* [Master's dissertation]. Federal University of Rio Grande do Sul (in Portuguese).

Charles, J.A., Earle, E.W., & Burford, D. (1978). The treatment and subsequent performance of cohesive fill left by opencast ironstone mining at Snatchhill experimental housing site, Corby. *Proceedings from the Clay Fills Conference, held at the Institution of Civil Engineers* (pp. 63-72). London: Institution of Civil Engineers.

Chow, Y.K., Yong, D.M., Yong, K.Y., & Lee, S.L. (1992). Dynamic compaction analysis. *Journal of Geotechnical Engineering*, 118(8), 1141-1157. https://doi.org/10.1061/(ASCE)0733-9410(1992)118:8(1141).

Consoli, N.C., Giese, D.N., Scheuermann Filho, H.C., Festugato, L., Rocha, M.M., Heineck, K.S., & Moreira, E.B. (2020). On porous bonded residual soil in natural and dynamically compacted states through plate load tests. *Journal of Geotechnical and Geoenvironmental Engineering*, 146(8), 1-8. https://doi.org/10.1061/(ASCE)GT.1943-5606.0002321.

Dalla Rosa, F. E., Ruver, C. A., & Thomé, A. (2004). Obtaining the resistance and deformability characteristics of a residual basalt soil through plate tests. *XXXI Jornadas Sud-Americanas Ingeniería Estructural* (pp. 1-12). Porto Alegre: Associação Sulamericana de Engenharia Estrutural.

Du, J., Shuaifeng, W., Sen, H., Yinqiu, Z., Hong, C., Yingqi, W. & Junwei, S. (2025). *D*ynamic response and densification mechanism of dynamic compaction for silt soil through a large-scale field test at Daxing Airport. *Soil Dynamics and Earthquake Engineering*, 190, 1-12.

Du, J., Wu, S., Hou, S., & Wei, Y. (2019). Deformation analysis of granular soils under dynamic compaction based on stochastic medium theory. *Mathematical Problems in Engineering*, 2019(1), 6076013. https://doi.org/10.1155/2019/6076013.

Faro, V.P. (2014). *Lateral loading on deep foundations associated with treated soil: design, load tests, and design guideline* [Doctoral thesis]. Federal University of Rio Grande do Sul (in Portuguese).

Fei, X.Z., Wang, Z., & Zhou, Z.B. (2002). Model test of improvement depth of dynamic compaction. *Journal of Sichuan University*, 34(4), 56-59.

Feng, S.J., Shui, W.H., Tan, K., Gao, L.Y., & He, L.H. (2011). Field evaluation of dynamic compaction on granular deposits. *Journal of Performance of Constructed Facilities*, 25(3), 241-249. https://doi.org/10.1061/(ASCE)CF.1943-5509.0000160.

Gambin, M.P. (1983). The Menard dynamic consolidation at Nice Airport. *Proceedings, 8th European Conference on Soil Mechanics and Foundation Engineering* (pp. 231-234). Helsinki: Balkema.

Ghanbari, E., & Hamidi, A. (2015). Improvement parameters in dynamic compaction to the slopes. *Journal of Rock Mechanics and Geotechnical Engineering*, 7(2), 233-236. https://doi.org/10.1016/j.jrmge.2015.02.002.

Hamidi, B. (2014). *Distinguished ground improvement projects by dynamic compaction or dynamic replacement* [Doctoral thesis]. Curtin University (in Portuguese).

Han, J. (2015). *Principles and practices of ground improvement*. Hoboken: John Wiley and Sons.

Kondner, R.L. (1963). Hyperbolic stress-strain response: cohesive soils. *Journal of the Soil Mechanics and Foundations Division*, 3429(1), 115-143. https://doi.org/10.1061/JSFEAQ.0000479.

Kondner, R.L., & Horner, J.M. (1965). Triaxial compression of a cohesive soil with effective octahedral normal stress control. *Canadian Geotechnical Journal*, 2(1), 40-52. https://doi.org/10.1139/t65-004.

Lee, F.H., & Gu, Q. (2004). Method for estimating dynamic compaction effect on sand. *Journal of Geotechnical and Geoenvironmental Engineering*, 130(2), 139-152. https://doi.org/10.1061/(ASCE)1090-0241(2004)130:2(139).

Leonards, G.A., Holtz, R.D., & Cutter, W.A. (1980). Dynamic compaction of granular soils. *Journal of the Geotechnical Engineering Division*, 106(1), 35-44. https://doi.org/10.1061/AJGEB6.0000914.

Li, J., Wang, W., Luo, L., Yao, X., & Hu, J. (2025). Evaluation of dynamic compaction load conversion methods and vibration reduction treatments. *Buildings*, 15(1), 1-19. https://doi.org/10.3390/buildings15010111.

López-Querol, S., Fernández-Merodo, J.A., Mira, P., & Pastor, M. (2007). Numerical modelling of dynamic consolidation on granular soils. *International Journal for Numerical and Analytical Methods in Geomechanics*, 32(12), 1431-1457. https://doi.org/10.1002/nag.676.

Lukas, R.G. (1995). *Dynamic compaction* (Geotechnical Engineering Circular, No. 1). Springfield: National Technical Information Service.

Luongo, V. (1992). Dynamic compaction: predicting depth of improvement. In: R. H. Borden, R. D. Holtz & I. Juran (Eds.), *Grouting soil improvement and geosynthetics* (ASCE Geotechnical Special Publication, No. 30, pp. 927-939). New York: American Society of Civil Engineers.

Mayne, P.W., Jones Juniot Jr, J.S., & Dumas, J.C. (1984). Ground response to dynamic compaction. *Journal of Geotechnical Engineering*, 110(6), 757-774. https://doi.org/10.1061/(ASCE)0733-9410(1984)110:6(757).

Mehdipour, S., & Hamidi, A. (2017). Impact of tamper shape on the efficiency and vibrations induced during dynamic compaction of dry sands by 3D finite element modelling. *Civil Engineering Infrastructures Journal*, 50(1), 151-163.

Menard, L., & Broise, Y. (1975). Theoretical and practical aspects of dynamic consolidation. *Geotechnique*, 25(1), 3-17. https://doi.org/10.1680/geot.1975.25.1.3.

Meneghetti, L.R.R., Thomé, A., Denardin, N., Girardello, V., & Berte, V.S. (2009). Aplicação em laboratório de técnicas de biorremediação em um solo residual contaminado com diesel e biodiesel. *Geotecnia*, 116(116), 83-98. https://doi.org/10.14195/2184-8394_116_5.

Mikasa, M., Takada, N., Ikeda, M., & Takeuchi, I. (1988). Centrifuge model test of dynamic consolidation. In *Proceedings of the International Conference on Geotechnical Centrifuge* (pp 185-192). Rotterdam: Balkema.

Mitchell, J.K. (1981). Soil improvement, state-of-the-art report. *Proceedings 10th International Conference on Soil Mechanics* (Vol. 4, No. 12, pp. 509-565) Stockholm: International Society for Soil Mechanics and. Geotechnical Engineering.

Moon, J.-S., Jung, H.S., Lee, S., & Kang, S.-T. (2019). Ground improvement using dynamic compaction in Sabkha deposit. *Applied Sciences*, 9(12), 1-16. https://doi.org/10.3390/app9122506.

Mostafa, K. (2010). *Numerical modelling of dynamic compaction in cohesive soils* [Doctoral thesis]. University Akron.

Nogami, J.S., & Villibor, D.F. (1995). *Pavimentação de baixo custo com solos lateríticos.* São Paulo: Arte & Ciência.

Oshima, A., & Takada, N. (1994) Effect of ram momentum on compaction by heavy tamping. In *Proceedings of the 13th International Conference Soil Mechanics Foundation Engineering* (pp. 1141-1144). New Delhi: Oxford & IBH Publishing.

Oshima, A., & Takada, N. (1997) Relation between compacted area and ram momentum by heavy tamping. In *Proceedings of the 14th International Conference Soil Mechanics Foundation Engineering* (pp. 1641-1644). Hamburg: A. A. Balkema.

Pan, J.L., & Selby, A.R. (2001). Analysis of dynamic compaction of loose soils under impact loads. In *4th International Conference on recent advances in Earthquake Engineering and Soil Dynamics*, San Diego. CA.

Qian, J.H. (1987). Dynamic consolidation: from practice to theory. In *Proceedings 8th Asian Regional Conference on Soil Mechanics and Foundation Engineering*, Kyoto.

Rizzon, M.M. (2016). *Efeitos da compactação dinâmica em solo residual* [Master thesis]. Federal University of Rio Grande do Sul (in Portuguese).

Rollins, K., & Kim, J. (2010). Dynamic compaction of collapsible soils based on U.S. case histories. *Journal of Geotechnical and Geoenvironmental Engineering*, 136(9), 1178-1186. https://doi.org/10.1061/(ASCE)GT.1943-5606.0000331.

Rollins, K.M., & Rogers, G.W. (1994). Mitigation measures for small structures on collapsible alluvial soils. *Journal of Geotechnical Engineering*, 120(9), 1533-1553. https://doi.org/10.1061/(ASCE)0733-9410(1994)120:9(1533).

Ruver, C.A. (2011). *Estudo do arrancamento de fundações em solos tratados com cimento* (Doctoral thesis]. Federal University of Rio Grande do Sul (in Portuguese).

Sachetti, A.S., Rojas, J.W.J., & Heineck, K.S. (2014). Caracterização geotécnica dos solos de Passo Fundo e Erechim Geológica da rocha de Passo Fundo. *Revista de Engenharia Civil da IMED*, 1(1), 11-17. https://doi.org/10.18256/2358-6508/rec-imed.v1n1p11-17.

Serviço Geológico do Brasil – SGB (2025). *Mapa Geológico do Rio Grande do Sul.* Brasília: SGB. Retrieved in June 15, 2025, from https://rigeo.sgb.gov.br/bitstream/doc/10301/2/Geologico_MDT.pdf

Slocombe, B.C. (2013). Dynamic compaction. In K. Kirsch, J. A. Bello, D. Arellano & A. Bouazza (Eds.), *Ground improvement* (2nd ed.). London: ICE Publishing.

Smoltczyk, U. (1983) Deep compaction: general report. In *Proceedings of the 8th European Conference on Soil Mechanics and Foundation Engineering* (pp. 1105–1116). Helsinki.

Souza Junior, T.F., & Pasqual, R.P.S. (2021). New method to predict crater depth obtained in dynamic compaction. *Geotechnical and Geological Engineering*, 39(5), 3891-3993. https://doi.org/10.1007/s10706-021-01726-x.

Souza Junior, T.F., Jesus, F.F.S., Ruver, C.A., Heineck, K.S., & Luz, C.C. (2019) Aplicação do método de classificação MCT ao solo coesivo friccional do município de Passo Fundo – RS. In *X Seminário de Engenharia Geotécnica do Rio Grande do Sul* (pp. 1-11), Santa Maria: ABMS.

Streck, E.V., Kampf, N., Dalmolin, R.S.D., Klamt, E., Nascimento, P.C., & Schneider, P. (2002). *Solos do Rio Grande do Sul*. Porto Alegre: Emater.

Thomé, A., Cecchin, I., Reginatto, C., Colla, L.M., & Reddy, K.R. (2017). Biostimulation and rainfall infiltration: influence on retention of biodiesel in residual clayey soil. *Environmental Science and Pollution Research International*, 24(10), 9594-9604. https://doi.org/10.1007/s11356-017-8670-9.

Van Impe, W.F. (1989). Soil improvement techniques and their evolution. Rotterdam: Balkema.

Varaksin, S. (1981). Recent development in soil improvement techniques and their practical applications. *Louis Menard*, 38/39, 7-32.

Wang, W., Chen, J., & Wang, J. (2017). Estimation method for ground deformation of granular soils caused by dynamic compaction. *Soil Dynamics and Earthquake Engineering*, 92, 266-278. https://doi.org/10.1016/j.soildyn.2016.09.015.

Wang, W., Feng, Q., & Yang, C. (2019). Investigation on the dynamic liquefaction responses of saturated granular soils due to dynamic compaction in coastal area. *Applied Ocean Research*, 89(1), 273-283. https://doi.org/10.1016/j.apor.2019.05.025.

Yasrobi, S.S., & Asghari, E. (2004). Dynamic compaction in Assalouyeh, Iran. *Proceedings 50th International Conference on Case Histories in Geotechnical Engineering* (pp. 13-17). Missouri: University of Science and Technology.